Influence of top water on SAGD steam chamber growth in heavy oil reservoirs An experimental study

Lyu, Xiaocong; Liu, Huiqing; Tian, Ji; Zheng, Qiang ; Zhao, Wei

DOI
10.1016/j.petrol.2021.109372

Publication date
2021

Document Version
Final published version

Published in
Journal of Petroleum Science and Engineering

Journal of Petroleum Science and Engineering 208 (2022) 109372

Contents lists available at ScienceDirect

Journal of Petroleum Science and Engineering

journal homepage: www.elsevier.com/locate/petrol

Influence of top water on SAGD steam chamber growth in heavy oil reservoirs: An experimental study

Xiaocong Lyu [a,*], Huiqing Liu [b], Ji Tian [c], Qiang Zheng [c], Wei Zhao [d]

[a] Department of Geoscience and Engineering, TU Delft, Delft, Netherlands
[b] State Key Laboratory of Petroleum Resources and Prospecting, China University of Petroleum, Beijing, China
[c] CNOOC Research Institute, Beijing, China
[d] China Petroleum Technology & Development Corporation, Beijing, China

ARTICLE INFO

Keywords:
Steam-assisted gravity drainage (SAGD)
Steam chamber
Top water
Heavy oil
Experiments

ABSTRACT

Steam-assisted gravity drainage (SAGD) is one efficient and mature technology for recovering heavy oil and bitumen resources. The key underlying mechanism is the growth of the steam chamber after injecting steam. However, due to the complex geological environment, the thief zones exist and have a prejudicial effect on the development of the steam chamber, thus impacting the ultimate heavy-oil recovery. In this work, our objective is to investigate the effect of a top-water thief zone (i.e., water zone overlies the oil sand) on SAGD performance and further to understand the crucial mechanisms that control the heat loss during steam injection. A large-scale three-dimensional experimental apparatus is used to carry out the SAGD process with a top aquifer. Based on the similarity criterion, the field-scale model is transformed into a laboratory elemental model. To evaluate the SAGD performance quantitatively, the dynamic growth of the steam chamber is measured using the thermal detectors and the production data is recorded. The results show that the steam chamber exhibits three distinguished stages, that is, upward spread, lateral extension, and downward development in the presence of top-water zone. The bottom-water zone has less impact on the steam-chamber growth. The existence of a confined top-water zone, however, significantly affects SAGD performance, especially the lateral expansion of the steam chamber. The lateral propagation of the steam front is hindered by the top thief zone due to the heat exchange with the top water. Once the steam chamber reaches the boundary, the accumulation of energy in the water thief zone, in turn, can reduce the remaining oil saturation along the topwater–oil interface. This study provides us some key insights into the development of heavy oil resources with top thief zones when implementing SAGD technology.

1. Introduction

Heavy oil and bitumen account for 2/3 of the total crude oil resources in the world. The effective development of these resources is very significant to the world energy supply (Butler, 1991; Edmunds et al., 1994). The viscosity of heavy oil or bitumen is sensitive to temperature variations, a thermal process, therefore, is usually applied to reduce the viscosity, thus improving the ultimate recovery. In practice, the hot steam is chosen and injected into the reservoir to heat the fluids. Application of steam injection technology has been proved to be the most commercially successful EOR technique for heavy-oil reservoirs (Friedmann et al., 1994; Patzek, 1996; Gotawala and Gates, 2008; Fatemi and Jamaloei, 2011; Lyu et al., 2018). Steam can be injected in three types, that is, steam flooding, cyclic steam stimulation (CSS) and steam-assisted gravity drainage (SAGD) with/without chemical agents (Butler, 1991; Speight, 2013; Pang et al., 2018; Dong et al., 2019; Liu et al., 2019).

SAGD technique has been successfully and widely used to improve heavy-oil recovery (Butler, 1991; Gates and Chakrabarty, 2006). This technique was first proposed by Butler et al. (1981), and then was extended by some researchers. The SAGD process contains two parallel horizontal wells (e.g., for injection and production, respectively) in reservoirs for oil recovery. The upper horizontal well is designed to inject high-temperature steam, while the heated oil and condensate water are produced from the bottom horizontal well (Gates et al., 2008; Hashemi-Kiasari et al., 2014). The steam with high temperature and low density rises upward and forms a steam chamber, leading to a significant reduction of oil viscosity. Thus the oil mobility increases by several orders of magnitude, then the oil drains down by gravity to lower horizontal well.

* Corresponding author.
E-mail address: x.lyu@tudelft.nl (X. Lyu).

https://doi.org/10.1016/j.petrol.2021.109372
Received 27 May 2021; Received in revised form 9 August 2021; Accepted 11 August 2021
Available online 17 August 2021

Some researchers have conducted numerous laboratory experiments or field pilots to understand the performance and corresponding mechanisms of SAGD processes. The effectiveness of two different configurations, i.e., horizontal-well-pair and the vertical-injection–horizontal-production, was discussed in Rose and Deo (1995). They found that the production of later scheme is around 40% of that of the horizontal-well-pair. The oil–steam ratio (OSR) is also comparable between the two strategies. Butler (2004) then investigated the effect of non-condensible gas on the growth of the steam chamber and proved that the accumulation of gas can be attractive because the lower heat conductivity of non-condensible gas can reduce the heat loss between steam and cap rock. The performance of SAGD strategy in a inclined oil-wet reservoir with heterogeneities and fractures was discussed in Hashemi-Kiasari et al. (2014) and the impact of operational parameters was also investigated through numerical simulations. All these studies, including theoretical, experimental, and numerical, have proved SAGD as a promising EOR process (Reis, 1990; Ito and Suzuki, 1996; Chan et al., 1997; Dusseault et al., 1998; Zhu et al., 2015).

To improve the SAGD performance further, some additives, such as solvent and air (or only nitrogen), may be added to mitigate the heat loss or overcome the geological formation complexity. In Table 1, a few studies on investigating the SAGD performance with different effects are listed. The addition of solvent can significantly reduce energy requirement, enhance produced oil quality, and improve oil recovery as well (Mohammadzadeh et al., 2010; Al-Muayri, 2012). In addition, noncondensable gases, such as carbon dioxide, nitrogen or methane, injected with steam, had been proved to be an effective way to improve the SAGD performance due to its low thermal conductivity, low interfacial tension, thermal expansion, low cost and availability (Canbolat et al., 2004; Rahnema et al., 2011; Yuan et al., 2018; Li et al., 2019). In these researches, a 2D physical model is usually used to study the development of the steam chamber without the effect of water thief zones.

Reservoir heterogeneity plays an important role in SAGD performance, because it is sensitive to the geological structure. In the presence of lean zones, SAGD performance is limited in oil sands reservoirs due to the increasing steam–oil ratio, leading to a reduction of the amount of oil recovered (Fairbridge et al., 2012). Doan et al. (2003) found that the existence of a water thief zone hinders the heavy-oil recovery in the SAGD process and one bottom-water layer has a less effect on recovery than the overlying water layer case through a commercial simulator. Some researchers investigated SAGD performance with the presence of thief zones, such as an overlying gas cap and top-water thief zone, in lab- and field-scale through reservoir simulations (Law et al., 2000; Pooladi-Darvish and Mattar, 2002; Nasr et al., 2003; Law et al., 2003). These studies found that the existence of those thief zones reduces the ultimate oil recovery significantly. Xu et al. (2014a,b) carried out some numerical studies to investigate how reservoir heterogeneity with lean zones affects SAGD performance and hybrid CSS/SAGD process in Long Lake in Canada. Through a scaling 3D experiment, Tian et al. (2016) analyzed the feasibility of SAGD process within the high-pressure environment and found that the high-pressure environment affect the SAGD process with a lower oil recovery.

Even though there are numerous numerical studies and field pilots on SAGD processes, relatively few efforts have been made towards the experimental investigation in the presence of the top-water thief zone, especially on a large scale, due to the difficulties in modeling the top-water zone. In our study, we use a 3D apparatus to study the SAGD process in the presence of a top-water thief zone and analyze the growth of the steam chamber. This facility can be rotated 360 degrees along the center axis, which simplifies the procedure to mimic the top-water thief zone. The paper is structured as follows. First, we briefly describe our experimental setup and the procedure to carry out the experiment. Next, we analyze the experimental results with a top-water thief zone in different periods. Then we compare and discuss the difference in the growth of the steam chamber in different formations. We end the paper up with a discussion and main conclusions.

2. Experimental setup

2.1. Apparatus

Fig. 1 shows the apparatus used in the experiment. It contains an injection–production system, a 3D sand model, and monitoring system. The injection–production system is used to generate and inject steam by a steam generator and an ISCO pump. To control and measure the rate of oil and water, a back-pressure regulator (BPR) and a hand pump are deployed in the outlet. In order to offset the heat exchange in the experiment, the injection lines are entangled by electric heating belts to keep a higher temperature. The main section is the 3D reservoir tank, which is made of stainless steel with an internal size of 40 cm in the three dimensions and rotates about a horizontal axis. To reduce heat loss, the internal wall is covered by insulated materials. The maximum endurable pressure and temperature are 80 bar and 350 °C, respectively. To maintain the reservoir temperature, the apparatus is placed into an incubator and is heated during the experiment. The real time data, such as pressure and temperature, are transmitted to the computer by pressure and temperature transducers instantaneously, then we can monitor and analyze the dynamic behavior of the steam chamber in the SAGD process.

2.2. Experimental design

The SAGD process is performed in the experiment using the oil sample (dead oil) from Long Lake region, Alberta, Canada. The initial reservoir temperature is only 7 °C due to the shallow depth of the deposit (300 m). The sand used in the experiment is 12 mesh quartz sand with good abrasion except for the water thief zone (finer sand). On the basis of the similarity criterion of thermal recovery (Law et al., 1993; Pang et al., 2015), the field parameters are transformed into laboratory parameters, as shown in Table 2. The detailed procedure can be found in A. During the experiment, some similarity criteria are relaxed, for instance, the length of a horizontal well. The designed well length is 320 cm; however, the internal size of the tank is 40 cm. Therefore, the length of wells is set as 40 cm, equal to the size of the equipment, corresponding to 1/8 of the designed total injection rate. Another one is the wellbore radius, which is scaled by controlling the denseness of perforation.

The oil sample is extra-heavy oil with super high viscosity, 500×10^4 mP s in reservoir condition. The oil sample has an API gravity of less than 10.0°. After the simulated distillation experiments, we found that the asphaltene content of the crude heavy oil is around = 13.50 wt% (n-hexane insoluble). The variation of oil viscosity with temperature is measured (Fig. 2). The oil viscosity is sensitive to temperature changes; therefore, once steam is injected, the reservoir temperature increases, leading to a sharp reduction of oil viscosity (i.e., higher oil mobility).

2.3. Procedure

After transforming reservoir parameters with similarity criteria to laboratory parameters, we carry out the experiments following two main steps. The first one is model preparation (Fig. 3):

- Firstly, washing and drying the selected sands. Before that, the porosity and permeability of the selected sands are already measured. Then the simulated oil and sands are mixed.
- Put the oil sand into the model step by step, and assemble pressure detectors, thermocouples and wells in assigned positions. The designed steam circulation well is similar to Tian et al. (2017). The sands saturated with water is placed at the bottom layer uniformly, then the model is filled with oil sands. Finally, we fill the model using clays which can bear high temperature.

Table 1
Laboratory researches on SAGD performance with different effects.

Author	Purpose	Model setup
Yang and Butler (1992)	Reservoir heterogeneity on SAGD performance	2D model
Canbolat et al. (2004)	Non-Condensable Gases on SAGD performance	Small 3D model
Mohammadzadeh et al. (2010)	Solvent-Aided SAGD process	2D model & pore-scale dimensions
Rahnema et al. (2011)	Air injection in SAGD chamber	2D model
Al-Muayri (2012)	Enhancing SAGD performance through solvent addition	2D partially-scaled physical model
Tian et al. (2017)	SAGD performance with high pressure environment	3D model
Yuan et al. (2018)	Nitrogen assisted SAGD	2D physical model
Li et al. (2019)	Nitrogen assisted SAGD	2D visual model
Wang et al. (2019)	Gas penetration through interlayer affects SAGD performance	2D visual model (Li et al., 2019)

Table 2
Conversion of field parameters to experimental parameters.

	Parameter	Field scale	Laboratory scale
Basic parameters	Wellbore radius	0.1 m	6 mm
	Well distance between injector and producer	10.0 m	4.0 cm
	Horizontal length	800 m	320 cm (40 cm)
	Distance between producer and bottom layer	3.0 m	1.2 cm
	Oil-layer thickness	23.0 m	9.2 cm
	Top water thickness	12.0 m	4.8 cm
	Porosity of oil zone	0.33	0.33
	Porosity of water zone	–	0.103
	Absolute permeability	5 μm^2	20 μm^2
	Initial oil saturation	0.684	1.0
	Oil viscosity at reservoir temperature	5×10^6 cp	5×10^6 cp
	Reservoir temperature	7 °C	7 °C
	Initial reservoir pressure	15 bar	15 bar
	Saturated steam temperature	225 °C	225 °C
	Saturated steam pressure	25 bar	25 bar
	Steam quality	0.8	0.8
SAGD process	Injection–production pressure difference	5 bar	0.02 bar
	Time	1 year	22.0 min
	Steam injection rate	300 t/day	30.0 mL/min

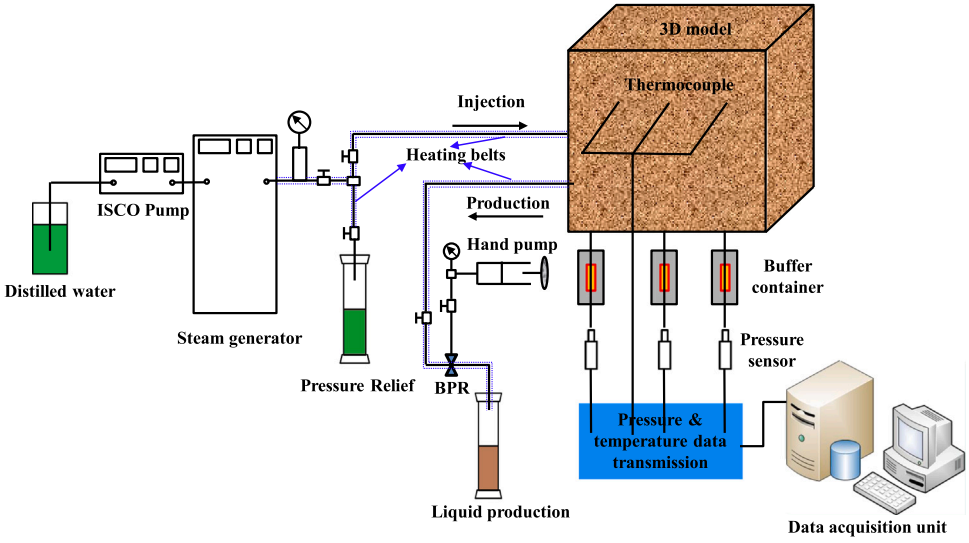

Fig. 1. 3D gravity drainage experiment apparatus.

- After packing the model, the nitrogen is injected into the model to check the hermeticity. After 24 h, if the pressure does not change, we do a rotation of 180°, then the bottom water layer moves to the top to mimic the top thief zone. We repeat the pressure checking process to guarantee the hermeticity.
- The 3D model is placed into the air bath. To keep the same reservoir condition, the temperature is set at reservoir temperature (7 °C) and is aged for 48 h.

Once the preparation is done, the model is placed into the air bath and the preheating process is carried out by using the steam circulation method. This process is terminated until the temperature between injector and producer exceeds 110 °C, which guarantees the inter-well region is heated thoroughly. After that, steam is injected at a constant rate continuously. Once the oil–steam ratio is below 0.1, the injection is terminated. In the process, both temperature and pressure data are recorded to monitor the development of the steam chamber.

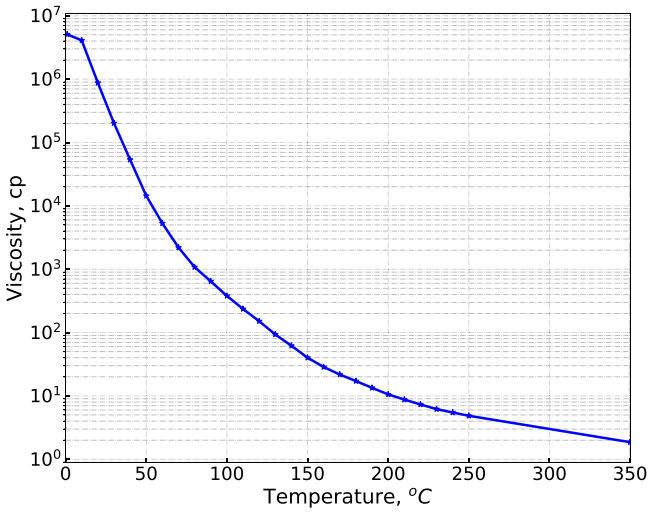

Fig. 2. Viscosity–temperature relationship of the oil sample used in the experiment.

3. Results and discussion

3.1. Preheating process

A preheating operation is required to establish thermal connection between the injector and producer before initiating the SAGD process. This operation can guarantee that the area between wells is heated thoroughly and oil can move to the bottom producer with gravity drainage in the later SAGD process. Fig. 4 exhibits the profiles of temperature variations in the preheating process at different times, i.e., different pore volume injection. Initially, the heating area around wells increases due to heat conduction with an ellipse-shape heating area (Fig. 4(a)). With increasing heat input, the heating area grows gradually and becomes the shape of a pear (Fig. 4(c)). High-temperature steam is injected from the bottom producer, as shown in Tian et al. (2017). When the steam flows to the upper injection well, the steam is cooled down to a relatively lower temperature. Then two heat sources with different temperatures are heating the top and bottom area. In a short period, the temperature around the bottom well is higher. Once the heat front reaches the bottom boundary, it expands laterally slowly and the area surrounding the producer is heated completely. After that, much heat is carried to the upper injector. With the increase of time, the injector and producer gradually build up the thermal communication.

As shown in Fig. 4, after the preheating process, the minimum temperature between the injector and the producer is above 110 °C, which indicates a good thermal communication between wells due to the significant reduction of oil viscosity compared to that under reservoir temperature (cf. Fig. 2). Note that the heat front (110 °C) is still far away from the top-water zone, then much oil is heated and produced before the water invades the steam chamber. The gravity-drainage process is activated with a designed steam injection rate continuously if the thermal communication is established. This stage is terminated once the oil–steam ratio is below 0.1.

3.2. Gravity-drainage process

Fig. 5 shows the variation of production data with time in the SAGD process. Three different phases can be distinguished: the oil rate increasing gradually, remaining stable with fluctuations, and decreasing finally. From the growth of the steam chamber, three periods can also be distinguished (Fig. 6 to 8), that is, upward spread, lateral growth, and downward propagation.

Fig. 6 displays the temperature profiles when the steam chamber expands upward. During this period, the steam chamber rises upward and grow gradually due to the low density of steam, corresponding to an increase of the oil rate (Fig. 5(a)) and oil–steam ratio (Fig. 5(b)). The high-temperature steam chambers also heat the surrounding oil, which causes the steam chamber relatively thinner. After 48 min (0.3 PV cold water equivalent (CWE)), the oil production rate reaches the peak (Fig. 5(a)), with period recovery is 4.1%, which indicates that the steam chamber arrives at the top-water zone (Fig. 6(c)). Fig. 5(a) also shows that the water cut decreases slightly. The heated oil with

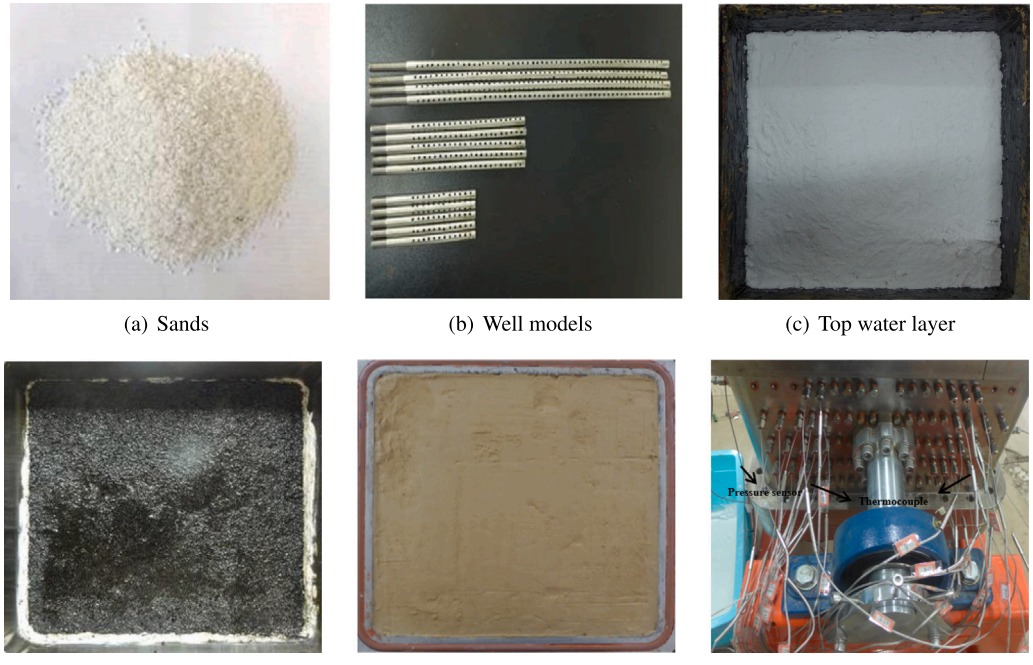

(a) Sands (b) Well models (c) Top water layer

(d) Oil sand layer (e) Top layer (f) Model setup

Fig. 3. Materials and the setup of the large-scale three-dimensional model.

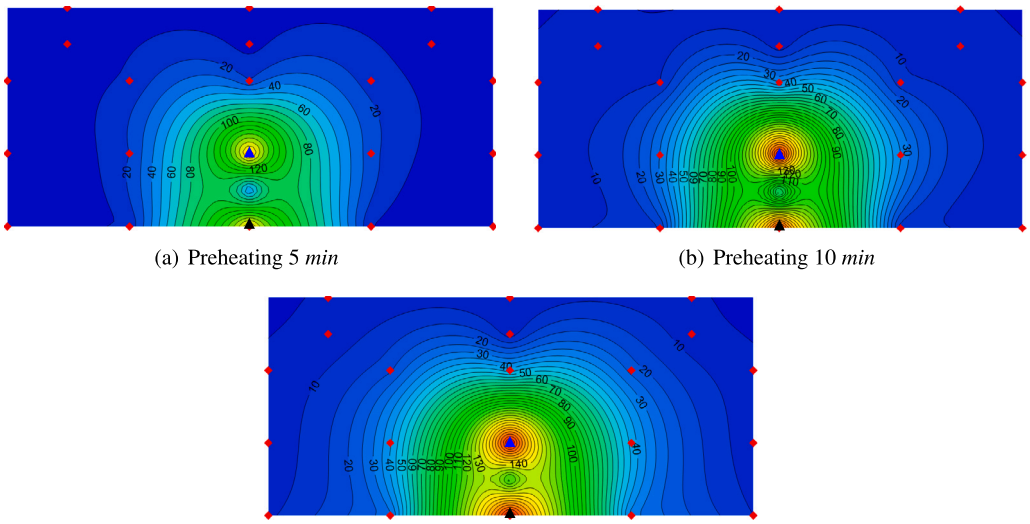

(a) Preheating 5 *min* (b) Preheating 10 *min*

(c) Preheating 15 *min*

Fig. 4. Temperature profiles of preheating process at different time. The black solid lines are isotherm. The symbols with red colors are the measured points where the thermocouple are located. The blue and black triangles are the injector and the producer, respectively. (For interpretation of the references to color in this figure legend, the reader is referred to the web version of this article.)

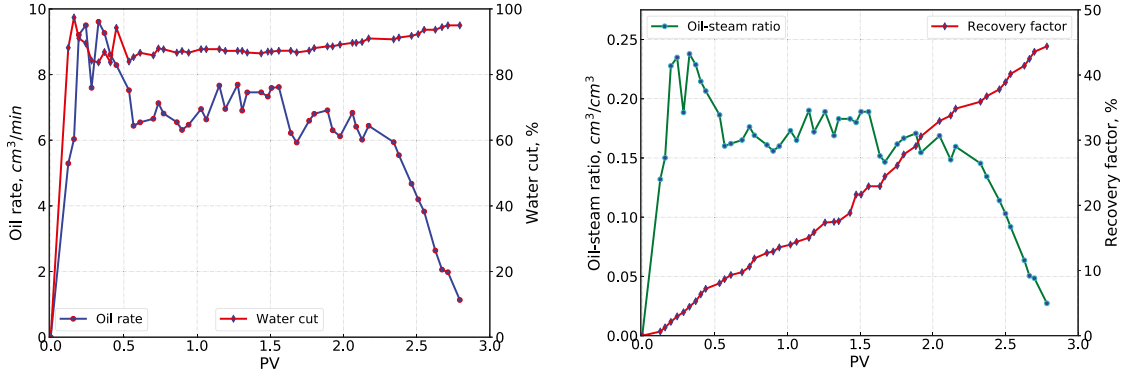

(a) Oil rate and water cut (b) Oil-steam ratio and recovery factor

Fig. 5. Production dynamic curves of the SAGD process.

lower viscosity moves to the producer, opening more space for steam expanding upward, thus less water is condensed.

Fig. 7 shows the lateral growth of the steam chamber. When the front reaches the top-water zone, the steam chamber expands laterally and heats the top water gradually. During this period, due to the high heat capacity of water, the temperature of the top layer increases slowly. It absorbs much heat and hinders the upward migration of steam. The speed of lateral expansion is much faster than that of vertical expansion, causing two triangles along the boundary of the oil zone and the top thief zone (Fig. 7(c)). The heated water then floods into the steam chamber, leading to a relatively lower-temperature steam front. Overall, the heated area is expanded significantly until the steam chamber front approaches the side boundary after 200 min (1.82 PV CWE).

The oil production rate and the oil–steam ratio remains stable during this period (Fig. 5), although there are some fluctuations. However, due to the invasion of cold top-water, the oil production rate slightly decreases, with increasing water-cut from 83.5% to 88.0% (Fig. 5(a)). Once cold water invades the steam chamber, the oil–steam ratio decreases because much steam is condensed to heat the top water. Although the oil in the steam chamber is still heated thoroughly, the total energy adsorbed by oil is reduced. The period oil recovery is increased by 29.4%, up to 33.5%, before the steam front touches the side boundary (Fig. 5(b)).

Fig. 8 demonstrates the downward propagation of the steam chamber after its front touches the side boundary. The top-water thief zone is heated further, leading to an increasing temperature there and relatively low temperature in the oil zone. When the SAGD process is terminated (oil–steam ratio below 0.1), the growth of the high-temperature steam chamber is limited (Fig. 8(b)). In this period, the oil rate and the oil–steam ratio decrease significantly, corresponding to an increasing water cut. The ultimate oil recovery is increased by 10.6%, compared to it in the lateral expansion process.

Fig. 9 illustrates the propagation of steam chamber in different directions. Once the high-temperature steam is injected into oil sand, it migrates upward and heats the heavy oil. With the injection of steam, the steam chamber rises gradually. Once the steam front reaches the water–oil interface (SAGD 48 min), the temperature gradient in the vertical direction starts to decrease (Fig. 9(a)). In this particular experiment, the rising rate of the steam chamber may be higher that in practice, because it stands for an overall average rise rate (Nasr et al., 2003). During this period, the heat of top-water zone is dominated mainly by heat conduction, corresponding to a small temperature gradient, as is illustrated in Fig. 9(a). The temperature of the top-water zone is around 120 °C. The lateral temperature along the water–oil interface is lower (Fig. 9(b)). The temperature around the steam chamber is relatively high, which causes a sharp change of temperature profile along with the water–oil contact.

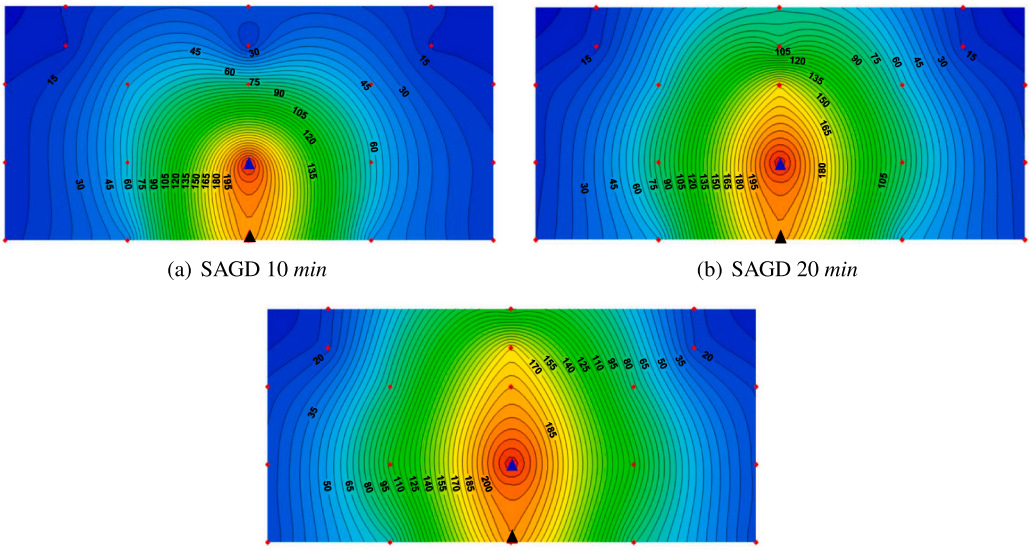

(a) SAGD 10 *min* (b) SAGD 20 *min*

(c) SAGD 48 *min*

Fig. 6. Temperature profiles of the SAGD process when the steam chamber rises upward. The black solid lines are isotherm. The symbols with red colors are the measured points where thermocouples are located. The blue and black triangles are the injector and the producer, respectively. (For interpretation of the references to color in this figure legend, the reader is referred to the web version of this article.)

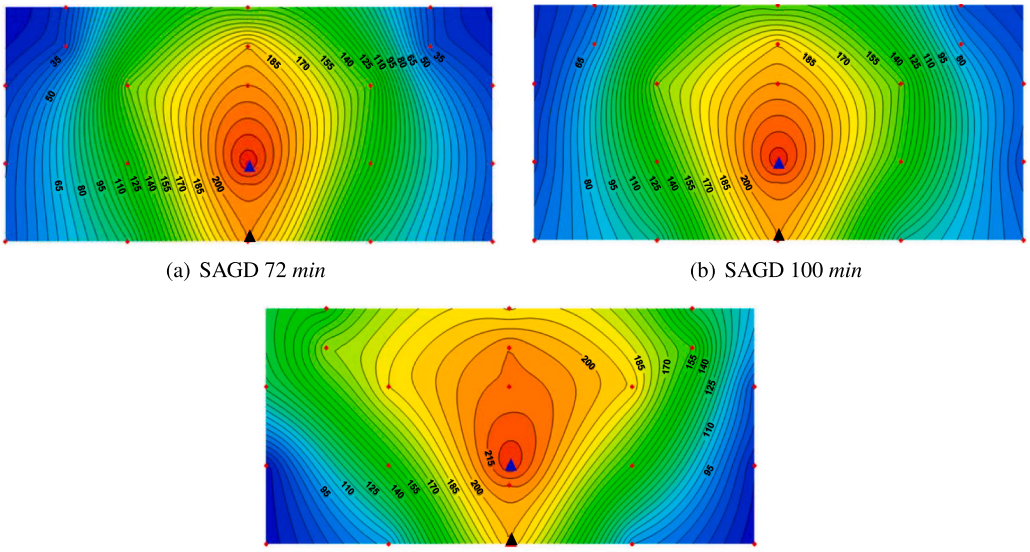

(a) SAGD 72 *min* (b) SAGD 100 *min*

(c) SAGD 200 *min*

Fig. 7. Temperature profiles of the SAGD process when the steam chamber expands laterally. The black solid lines are isotherm. The symbols with red colors are the measured points where thermocouples are located. The blue and black triangles are the injector and the producer, respectively. (For interpretation of the references to color in this figure legend, the reader is referred to the web version of this article.)

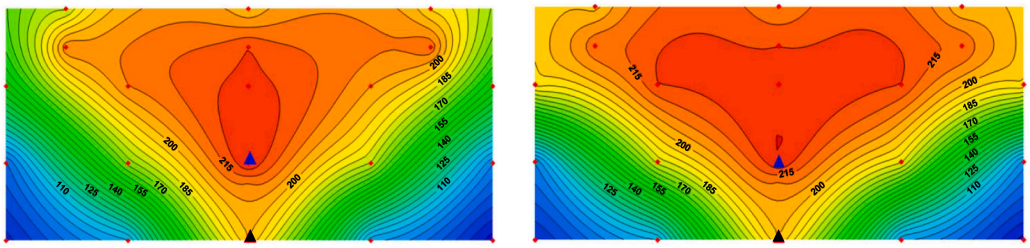

(a) SAGD 300 *min* (b) SAGD 450 *min*

Fig. 8. Temperature profiles of the SAGD process when the steam chamber expands downward. The black solid lines are isotherm. The symbols with red colors are the measured points where thermocouples are located. The blue and black triangles are the injector and the producer, respectively. (For interpretation of the references to color in this figure legend, the reader is referred to the web version of this article.)

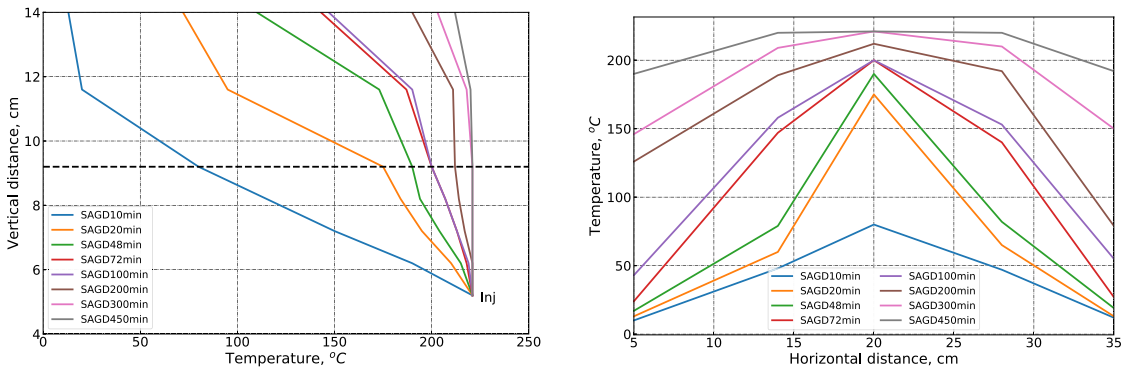

(a) Vertical (b) Water-oil contact

Fig. 9. The temperature profile in vertical and horizontal directions at different time. (a) The temperature profile right above the injector, and the black dashed line is the boundary of the top-water zone and oil zone. (b) The temperature profile along the water–oil contact (black line in (a)). (For interpretation of the references to color in this figure legend, the reader is referred to the web version of this article.)

After 72 min of steam injection, the high-temperature steam penetrates into the top-water zone at a distance of around 3.5 cm. The top-water zone is heated by the steam front, and due to heat dissipation with heat conduction, the front temperature is relatively low. Meanwhile, this process continues with continuously injecting hot steam. When the high-temperature steam front reaches the side boundary, it penetrates the whole top layer. However, the lateral heated area of the top-water zone is limited (Fig. 9(b)). The temperature of the margin is relatively low compared to that in the middle of the model. Following 450 min of steam injection, the steam chamber does not propagate upward significantly; instead, the margin of the model is gradually heated in both the top-water zone and oil sand zone.

3.3. Growth of steam chamber in different water thief zones

Considering the complexity and time cost of this large-scale experiment, we simply compared our results with some previous researches qualitatively. Tian et al. (2016, 2017) already carried out a similar 3D experiment to investigate the effect of bottom water on the growth of the steam chamber. This is a good reference for the comparison, even though some parameters are different. Fig. 10 shows the propagation of the steam front at different times with the presence of bottom water. There are also three distinguished stages, i.e., upward expansion, lateral expansion, and downward expansion. Some visible differences, however, are existent in these two cases.

Fig. 10(a) and Fig. 6(c) show the temperature profile when the steam-chamber front reaches the top layer and oil–water contact, respectively. Both cases show similar behavior. During this period, the injected steam migrates upward and the heat loss into the top-water thief zone is dominated by the conduction; the top-water thief zone, therefore, has less impact on the growth of the steam chamber. Meanwhile, the top water mitigates the heat transition of steam and the caprock, which is beneficial to the lateral growth of the steam chamber. However, due to the higher conductivity of the caprock compared to the top-water, much heat is transferred into the caprock, leading to a relatively limited heated area.

Once the top-water penetrates into the steam chamber, with the continuous steam injection, the top-water significantly affects the propagation of the steam front (Fig. 10(b) and Fig. 7(c)). Heat exchange between the high-temperature steam and low-temperature top-water reduces the energy for heating the heavy oil, thus the lateral spread of the steam front is restricted. However, in heavy-oil reservoirs with the presence of bottom-water aquifer, the development of the steam chamber follows the conventional mode (Butler, 1991), i.e., the bottom water only adsorbs the energy by conduction.

There are big differences when the steam front arrives at the side boundaries of the model (see in Fig. 10(c) and Fig. 8(b)). The boundaries hinder the lateral expansion of the steam chamber. In the bottom-water reservoir, the steam chamber expands downward gradually and heats the oil region continuously. However, the top-water thief zone allows the steam to penetrate into the aquifer first. Due to the gravity override, the steam chamber starts to grow downward until the high-temperature steam fills in the top-water zone. Therefore, the presence of the top-water thief zone changes the shape and size of the steam chamber. With the same pore volume injection, the ultimate oil recovery in case where the top-water thief zone is present is around 44.1%, decreased by 8.7% compared with that of the bottom-water zone.

Fig. 11 schematically shows the final state of the steam chamber. In the presence of the top-water thief zone, once the steam front heats the oil–water interface, the water starts to flood into the steam chamber, further flows into the producer. This process prolongs the time of lateral expansion. Due to the confined volume of the aquifer, the steam gradually invades and occupies the whole thief zone, which, in turn, heats the remaining oil at the boundaries. Therefore, the heating area beneath the top-water thief zone is relatively larger and does not exhibit the conventional shape (Fig. 8(b)). However, the steam chamber shows a triangular shape in the bottom-water reservoir. This triangular steam chamber cannot heat the boundary thoroughly, leaving much oil at the boundaries (Fig. 10(c)).

4. Summary and discussion

In this work, we investigate and analyze the effect of different water thief zones on SAGD performance through a large-scale 3D model. By monitoring the temperature data during the experiment, the development of the steam chamber and the effect of water thief zones can be tracked and evaluated successfully. However, there are still some limitations which need to be resolved in future research:

(1) A relatively small pressure difference between overlying thief zone and the steam chamber can be distinguished in this experiment. This operation does not limit the migration of oil into the top-water zone (Nasr et al., 2003). However, it is a challenging task to quantitatively measure the oil loss into the top thief zone.
(2) During the preparation process, the location of these thermocouples and pressure sensors may change, which adds some uncertainties to the results. This issue is not easy to avoid because once we start to carry out the experiment, it is not possible to re-open the apparatus and change thermocouples. We need to find a flexible way to reduce the effect of this manual factor.

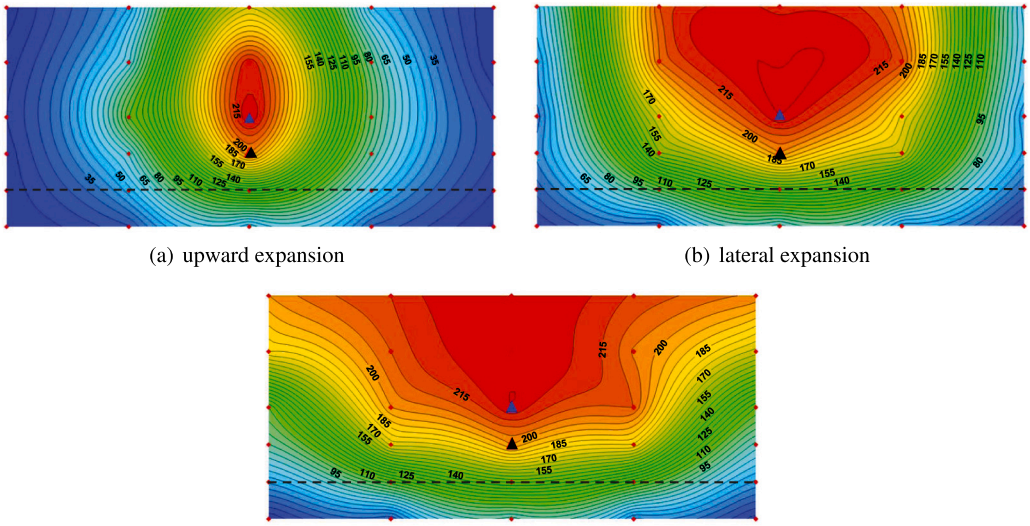

(a) upward expansion (b) lateral expansion

(c) downward expansion

Fig. 10. Temperature profiles of the SAGD process in the presence of bottom aquifer. The black solid lines are isotherm and the black dashed line is the water–oil contact. The symbols with red colors are the measured points where thermocouples are located. The blue and black triangles are the injector and the producer, respectively. (For interpretation of the references to color in this figure legend, the reader is referred to the web version of this article.)

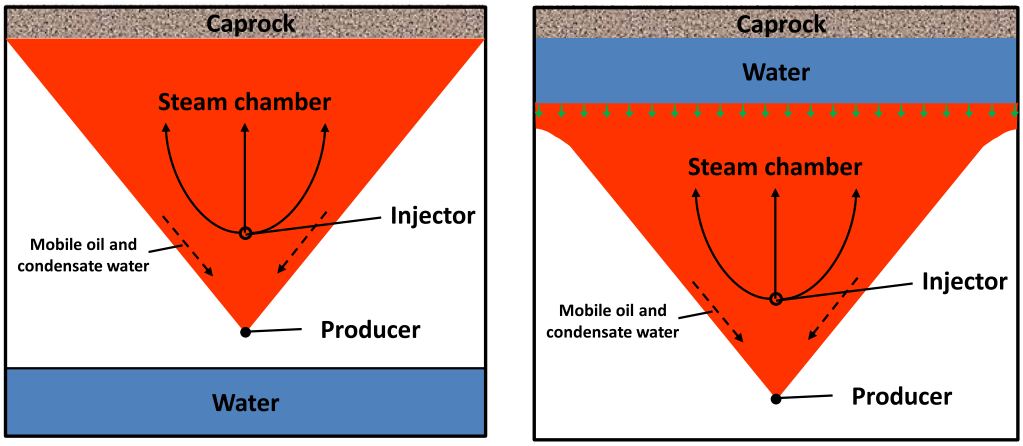

(a) Bottom water (b) Top water

Fig. 11. Schematic diagram of the steam chamber with different water thief zones.

(3) When we clean the model after the experiment, we found that the water exists in the gap between the oil sands and the inner wall of the tank, which indicates that the condensate water can migrate downward along this gap once the steam front reaches the boundaries. It may affect the final temperature distribution.

Although there are some uncertainties in this experiment, we strictly follow the designed procedure to complete all the steps and eliminate the possible errors in the experiment. Therefore, this is a good reference to help us design the SAGD applications with complicated thief zones.

In addition, to inhibit the breakup of the top-water zone, non-condensable gases, for instance, nitrogen, can be injected together with steam because these gases experience no apparent condensation phenomena and then exist stably above the steam chamber. It plays a role as an insulating layer that can reduce the heat conduction between the steam chamber and top-water zone. Considering the thickness of the top-water zone, another feasible technique, in theory, is the separate layer production where the top water is extracted firstly and afterward the steam is injected into the bottom layer to heat the heavy oil. However, this approach may increase the amount of steam because the steam needs to fill the empty water zone when it reaches the interface.

5. Conclusions

Based on the experimental results, we compare and analyze the effect of different water thief zones on the propagation of the steam chamber, and the following conclusions can be made:

- The whole SAGD process can be separated into three different stages, i.e., upward expansion, lateral expansion, and downward expansion, both within the presence of bottom- and top-water zones.
- Compared to the bottom-water zone, the existence of a confined top-water zone has a detrimental effect on SAGD performance and significantly affects the development of the steam chamber.
- The top water can reduce the remaining oil saturation along with the water–oil contact once the steam chamber reaches the boundary due to the high-temperature top water.

CRediT authorship contribution statement

Xiaocong Lyu: Experimental design, Carry out the experiments, Data analysis, Writing – review & editing. **Huiqing Liu:** Experimental

design, Supervision, Writing – review & editing. **Ji Tian:** Supervision, Writing – review & editing. **Qiang Zheng:** Supervision, Writing – review & editing. **Wei Zhao:** Experimental design, Writing – review & editing.

Declaration of competing interest

The authors declare that they have no known competing financial interests or personal relationships that could have appeared to influence the work reported in this paper.

Acknowledgments

This study was funded by National Science and Technology Major Project of China (2016ZX05031-003-004), Research Funds of China University of Petroleum (Beijing) (No. 2462020YXZZ032), and the China Scholarship Council (No. 201706440023).

Appendix A. Study of scaling criterion for SAGD process

A.1. Fundamental equations

In order to simulate the horizontal well reasonably in physical experiments, the fluids flow in porous media and in horizontal well needs to be considered together. The detailed description for horizontal-well scaling can be found in Pang et al. (2015). In this work, we describe the scaling process for SAGD process.

As shown in Fig. A.12, the reservoir thickness is h with the initial temperature T_R. The length of horizontal well is w, and the steam temperature is T_s. The hot steam condensates along the interface with an angle θ between the interface and horizontal line. The temperature of the interface is T_s. In SAGD process, the heat is transferred from steam chamber to the reservoir where temperature is relatively low. With the loss of energy, the temperature decreases in the reservoir. Assuming that the oil viscosity is μ and the kinetic viscosity is $\gamma_o(\gamma_o = \frac{\mu_o}{\rho_o})$ in a distance dl from the interface, the oil flux based on Darcy's law is then expressed as:

$$dq = \frac{Kg(\rho_o - \rho_g)sin\theta}{\mu_o}dl = \frac{Kgsin\theta}{\gamma_o}dl, \tag{A.1}$$

where K and g are absolute permeability and gravity acceleration; ρ_o and ρ_g are oil and steam density, respectively.

The phase potential is $(\rho_o - \rho_g)gsin\theta$, and compared to ρ_o, ρ_g is very small and can be ignored. Assuming that only heat conduction is present along the interface with a velocity U, the temperature of interface front under steady displacement is expressed as:

$$\frac{T - T_R}{T_S - T_R} = e^{-\frac{Ul}{a}}. \tag{A.2}$$

After derivation on both side:

$$dl = -\frac{a}{U}\frac{dT}{T_S - T_R}, \tag{A.3}$$

where T_R and T_S are initial reservoir temperature and steam temperature. U is the velocity of interface, and a is the rock heat conductivity.

If the reservoir is not heated, the flux can be expressed as:

$$dq_r = \frac{Kgsin\theta}{\gamma_R}dl. \tag{A.4}$$

Combining Eq. (A.1) and (A.4), the increased flux caused by the heat is:

$$dq_h = dq - dq_r = Kgsin\theta(\frac{1}{\gamma} - \frac{1}{\gamma_R})dl, \tag{A.5}$$

$$q_h = Kgsin\theta\int_0^\infty(\frac{1}{\gamma} - \frac{1}{\gamma_R})dl, \tag{A.6}$$

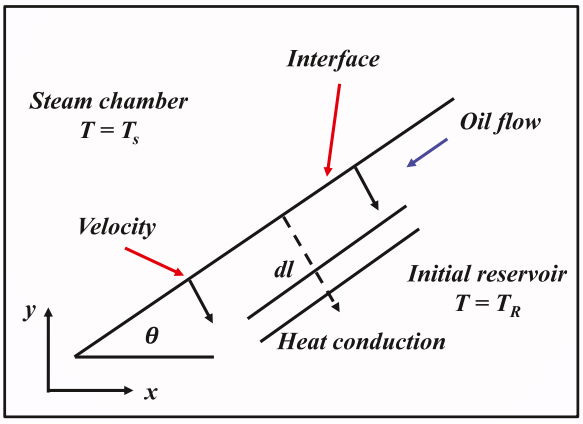

Fig. A.12. Schematic vertical section of the interface between steam chamber and reservoir.

where q, q_r, q_h are total flux, reservoir flux and increased flux, respectively.

If $1/\gamma_R \approx 0$:

$$\frac{\gamma_s}{\gamma} = (\frac{T - T_R}{T_S - T_R})^m, \tag{A.7}$$

where γ_s is the oil kinetic viscosity with steam temperature, and m is the dimensionless coefficient of the viscosity–temperature relationship.

Integrating Eq. (A.3) and (A.7):

$$\begin{aligned}\int_0^\infty(\frac{1}{\gamma} - \frac{1}{\gamma_R}) &= \int_0^\infty(\frac{1}{\gamma_s}\frac{T - T_R}{T_S - T_R})^m - (\frac{1}{\gamma_R})dl \\ &= \int_{T_R}^{T_S}(\frac{1}{\gamma_s}\frac{T - T_R}{T_S - T_R})^m - (\frac{1}{\gamma_R})\frac{a}{U}\frac{dT}{T_S - T_R} = \frac{a}{U}\frac{1}{m\gamma_s}.\end{aligned} \tag{A.8}$$

A.2. Oil flow rate

Based on material balance, the relationship between oil flow rate q and the front velocity in a tiny volume can be expressed as:

$$(\frac{\partial q}{\partial x})_t = \phi\Delta S_o(\frac{\partial y}{\partial t})_x, \tag{A.9}$$

where ϕ is the porosity and ΔS_o is the mobile oil saturation. The velocity along the interface is:

$$U = -cos\theta(\frac{\partial y}{\partial t})_x, \tag{A.10}$$

$$q = -\frac{Kgasin\theta}{m\gamma_s cos\theta(\partial y/\partial t)}, \tag{A.11}$$

$$\int_0^q = \int_0^{h-y}\frac{\phi\Delta S_o Kga}{m\gamma_s}dy, \tag{A.12}$$

$$q = \sqrt{\frac{2\phi\Delta S_o Kga(h - y)}{m\gamma_s}}. \tag{A.13}$$

At the bottom of the steam chamber (y=0), the oil rate is $\sqrt{\frac{2\phi\Delta S_o Kgah}{m\gamma_s}}$ which is a function of the height of steam chamber. It is not dependent on the shape of interface and the lateral growth of steam chamber.

A.3. Lateral velocity of the interface

The lateral velocity is defined as:

$$(\frac{\partial x}{\partial t})_y = \frac{-(\frac{\partial y}{\partial t})_x}{(\frac{\partial y}{\partial t})_t}, \tag{A.14}$$

$$(\frac{\partial x}{\partial t})_y = \sqrt{\frac{Kga}{2\phi\Delta S_o m\gamma_s(h - y)}}. \tag{A.15}$$

Table A.3
Dimensionless scaling groups for SAGD process design.

Scaling groups	Physical significances	Prototype
$B_3 = \sqrt{\frac{Kgh}{a\phi\Delta S_o m\gamma_s}}$	SAGD dimensionless parameter	Key parameter for SAGD similarity
$t_D = \frac{t}{h}\sqrt{\frac{Kga}{\phi\Delta S_o m\gamma_s h}}$	Dimensionless time	Production time
$q_s = \omega\sqrt{\frac{2Kga\phi h}{m\gamma_s}}$	Ratio of steam injection rate	Steam injection rate

The lateral velocity is a function of vertical depth, and not depends on time. Assuming that the shape of the steam chamber is a vertical plane above the producer, the lateral moving distance of the steam chamber is a function of time t and height y:

$$x = t\sqrt{\frac{Kga}{2\phi\Delta S_o m\gamma_s(h-y)}}. \tag{A.16}$$

Finally we can obtain the moving distance of the steam chamber in vertical direction:

$$y = h - \frac{Kga}{2\phi\Delta S_o m\gamma_s(h-y)}(\frac{t}{x})^2. \tag{A.17}$$

A.4. Steam injection rate

To maintain a stable steam chamber, the steam injection rate of prototype and model should be exactly same. Assuming that after dt, the interface between the steam chamber and reservoir moves a distance dx from the injector, and the total steam injection volume is:

$$Q_s = 2h\omega\phi dx, \tag{A.18}$$

where Q_s is the steam injection volume, and ω is the perforation length of the horizontal well.

The steam injection rate is:

$$\frac{Q_s}{dt} = 2h\omega\phi\frac{dx}{dt}. \tag{A.19}$$

Then the velocity of hot fluids can be obtained:

$$(\frac{\partial x}{\partial t})_y = \sqrt{\frac{Kga}{2\phi m\gamma_s(h-y)}}. \tag{A.20}$$

At the bottom of the steam chamber where y=0:

$$\frac{Q_s}{dt} = 2h\omega\phi\sqrt{\frac{Kga}{2\phi m\gamma_s h}}, \tag{A.21}$$

$$q_s = \omega\sqrt{\frac{2Kga\phi h}{m\gamma_s}}. \tag{A.22}$$

Therefore, to keep the similarity of steam-chamber growth, the steam injection rate should satisfy the scaling criteria, as shown in Table A.3.

References

Al-Muayri, M.T., 2012. Experimental Investigation of Expanding Solvent Steam Assisted Gravity Drainage Using Multicomponent Solvents. Graduate Studies.

Butler, R.M., 1991. Thermal Recovery of Oil and Bitumen. Old Tappan, NJ (United States); Prentice Hall Inc..

Butler, R., 2004. The behaviour of non-condensible gas in SAGD-a rationalization. J. Can. Pet. Technol. 43 (01).

Butler, R., McNab, G., Lo, H., 1981. Theoretical studies on the gravity drainage of heavy oil during in-situ steam heating. Can. J. Chem. Eng. 59 (4), 455–460.

Canbolat, S., Akin, S., Polikar, M., 2004. Evaluation of SAGD performance in the presence of non-condensable gases. In: Canadian International Petroleum Conference. OnePetro.

Chan, M., Fong, J., Leshchyshyn, T., 1997. Effects of well placement and critical operating conditions on the performance of dual well sagd well pair in heavy oil reservoir. In: Latin American and Caribbean Petroleum Engineering Conference. Society of Petroleum Engineers.

Doan, L., Baird, H., Doan, Q., Ali, S., 2003. Performance of the SAGD process in the presence of a water sand-a preliminary investigation. J. Can. Pet. Technol. 42 (01).

Dong, X., Liu, H., Chen, Z., Wu, K., Lu, N., Zhang, Q., 2019. Enhanced oil recovery techniques for heavy oil and oilsands reservoirs after steam injection. Appl. Energy 239, 1190–1211.

Dusseault, M.B., Geilikman, M.B., Spanos, T., 1998. Heavy oil production from unconsolidated sandstones using sand production and SAGD. In: SPE International Oil and Gas Conference and Exhibition in China. Society of Petroleum Engineers.

Edmunds, N., Kovalsky, J., Gittins, S., Pennacchioli, E., 1994. Review of phase A steam-assisted gravity-drainage test. SPE Reserv. Eng. 9 (02), 119–124.

Fairbridge, J.K., Cey, E., Gates, I.D., 2012. Impact of intraformational water zones on SAGD performance. J. Pet. Sci. Eng. 82, 187–197.

Fatemi, S.M., Jamaloei, B.Y., 2011. Preliminary considerations on the application of toe-to-heel steam flooding (THSF): Injection well–producer well configurations. Chem. Eng. Res. Des. 89 (11), 2365–2379.

Friedmann, F., Smith, M., Guice, W., Gump, J., Nelson, D., 1994. Steam-foam mechanistic field trial in the midway-sunset field. SPE Reserv. Eng. 9 (04), 297–304.

Gates, I., Chakrabarty, N., 2006. Optimization of steam assisted gravity drainage in McMurray reservoir. J. Can. Pet. Technol. 45 (09).

Gates, I.D., Larter, S.R., Adams, J.J., Snowdon, L., Jiang, C., 2008. Preconditioning methods to improve SAGD performance in heavy oil and bitumen reservoirs with variable oil phase viscosity. In: International Thermal Operations and Heavy Oil Symposium. Society of Petroleum Engineers.

Gotawala, D.R., Gates, I.D., 2008. Steam fingering at the edge of a steam chamber in a heavy oil reservoir. Can. J. Chem. Eng. 86 (6), 1011–1022.

Hashemi-Kiasari, H., Hemmati-Sarapardeh, A., Mighani, S., Mohammadi, A.H., Sedaee-Sola, B., 2014. Effect of operational parameters on SAGD performance in a dip heterogeneous fractured reservoir. Fuel 122, 82–93.

Ito, Y., Suzuki, S., 1996. Numerical simulation of the SAGD process in the hangingstone oil sands reservoir. In: Annual Technical Meeting. Petroleum Society of Canada.

Law, D., Nasr, T., Good, W., 2000. Lab-scale numerical simulation of SAGD process in the presence of top thief zones: a mechanistic study. In: Canadian International Petroleum Conference. Petroleum Society of Canada.

Law, D.H., Nasr, T.N., Good, W.K., 2003. Field-scale numerical simulation of SAGD process with top-water thief zone. J. Can. Pet. Technol. 42 (08).

Law, D., Ridley, R., Kimber, K., 1993. Steam-foam drive experiments in one-eighth of a five-spot pattern. In: Technical Meeting/Petroleum Conference of the South Saskatchewan Section. Petroleum Society of Canada.

Li, S., Yu, T., Li, Z., Zhang, K., 2019. Experimental investigation of nitrogen-assisted SAGD in heavy-oil reservoirs: A two-dimensional visual analysis. Fuel 257, 116013.

Liu, Y., Iglauer, S., Cai, J., Amooie, M.A., Qin, C., 2019. Local instabilities during capillary-dominated immiscible displacement in porous media. Capillarity 2 (1), 1–7.

Lyu, X., Liu, H., Pang, Z., Sun, Z., 2018. Visualized study of thermochemistry assisted steam flooding to improve oil recovery in heavy oil reservoir with glass micromodels. Fuel 218, 118–126.

Mohammadzadeh, O., Rezaei, N., Chatzis, I., 2010. Pore-level investigation of heavy oil and Bitumen recovery using solvent- aided steam assisted gravity drainage (SA-SAGD) process. Energy Fuels 24 (12), 6327–6345.

Nasr, T., Law, D., Beaulieu, G., Golbeck, H., Korpany, G., Good, W., 2003. SAGD Application in gas cap and top water oil reservoirs. J. Can. Pet. Technol. 42 (01).

Pang, Z., Liu, H., Zhu, L., 2015. A laboratory study of enhancing heavy oil recovery with steam flooding by adding nitrogen foams. J. Pet. Sci. Eng. 128, 184–193.

Pang, Z., Lyu, X., Zhang, F., Wu, T., Gao, Z., Geng, Z., Luo, C., 2018. The macroscopic and microscopic analysis on the performance of steam foams during thermal recovery in heavy oil reservoirs. Fuel 233, 166–176.

Patzek, T.W., 1996. Field applications of steam foam for mobility improvement and profile control. SPE Reserv. Eng. 11 (02), 79–86.

Pooladi-Darvish, M., Mattar, L., 2002. SAGD Operations in the presence of overlying gas cap and water layer-effect of shale layers. J. Can. Pet. Technol. 41 (06).

Rahnema, H., Barrufet, M., Mamora, D., 2011. Experimental study of air injection in SAGD chamber. In: Canadian Unconventional Resources Conference. OnePetro.

Reis, J., 1990. Oil recovery mechanisms in fractured reservoirs during steam injection. In: SPE/DOE Enhanced Oil Recovery Symposium. Society of Petroleum Engineers.

Rose, P., Deo, M., 1995. Steam-assisted gravity drainage in oil sand reservoirs using a combination of vertical and horizontal wells. Fuel 74 (8), 1180–1184.

Speight, J.G., 2013. Heavy Oil Production Processes. Gulf Professional Publishing.

Tian, J., Liu, H., Pang, Z., 2017. A study of scaling 3D experiment and analysis on feasibility of sagd process in high pressure environment. J. Pet. Sci. Eng. 150, 238–249.

Tian, J., Liu, H., Pang, Z., Liu, H., Lv, X., Zhao, W., Wu, Y., Bai, J., Dong, M., 2016. Experiment and simulations of steam flooding in offshore heavy oil reservoir with bottom water. In: SPE Trinidad and Tobago Section Energy Resources Conference. Society of Petroleum Engineers.

Wang, Z., Li, Z., Sarma, H.K., Xu, Y., Wu, P., Yang, J., Wang, H., Lu, T., 2019. A visualization experimental study on gas penetration through interlayer to improve SAGD performance. J. Pet. Sci. Eng. 177, 959–970.

Xu, J., Chen, Z.J., Cao, J., Li, R., et al., 2014a. Numerical study of the effects of lean zones on SAGD performance in periodically heterogeneous media. In: SPE Heavy Oil Conference-Canada. Society of Petroleum Engineers.

Xu, J., Chen, Z.J., Yu, Y., Cao, J., et al., 2014b. Numerical thermal simulation and optimization of hybrid CSS/SAGD process in long lake with lean zones. In: SPE Heavy Oil Conference-Canada. Society of Petroleum Engineers.

Yang, G., Butler, R., 1992. Effects of reservoir heterogeneities on heavy oil recovery by steam-assisted gravity drainage. J. Can. Pet. Technol. 31 (08).

Yuan, Z., Liu, P., Zhang, S., Li, X., Shi, L., Jin, R., 2018. Experimental study and numerical simulation of nitrogen-assisted SAGD in developing heavy oil reservoirs. J. Pet. Sci. Eng. 162, 325–332.

Zhu, L., Zeng, F., Huang, Y., 2015. A correlation of steam chamber size and temperature falloff in the early-period of the SAGD process. Fuel 148, 168–177.